Eng. Sci., 2022, **19**, 301–311

Engineered Science

DOI: https://dx.doi.org/10.30919/es8e735

Hydrophobic and Antimicrobial Polyimide Based Composite Phase Change Materials with Thermal Energy Storage Capacity, Applied as Multifunctional Construction Material

Mengman Weng,[1] Shengdong Liu,[1] Jingtao Su,[1] Weihao Xu,[1] Jintao Huang,[1, 2,*] Wanyi Tan,[1] Yidong Liu[1] and Yonggang Min[1,*]

Abstract

In recent years, it is important to develop efficient multifunctional construction materials under building energy consumption increased continuously. In this study, paraffin/polyimide aerogel composite phase change materials (CPCM) with excellent thermal management and hydrophobic thermal insulation by simple melt impregnation method were prepared. Among them, P-$P_{75}O_{25}$ ($n_{(BPDA\text{-}PPD)}$:$n_{(BPDA\text{-}ODA)}$ = 75:25) CPCM shows excellent comprehensive performance. Its latent heats are 100.98 J/g and 96.21 J/g and enthalpy efficiency is 93.52% and 92.31% during the melting and freezing process, respectively. After 200 thermal cycles, the enthalpy loss rate of melting and freezing is 4.25% and 0.73%. At the same time, superior hydrophobic and antimicrobial resistance is verified. All results indicate that P-$P_{75}O_{25}$ has great potential as a green construction material.

Keywords: Polyimide aerogel; Composite phase change material; Thermal energy storage; Hydrophobic; Antimicrobial resistance.
Received: 28 April 2022; Revised: 25 May 2022; Accepted: 27 May 2022.
Article type: Research article.

1. Introduction

Nowadays, building energy consumption increased continuously with the improvement of people's living comfort.[1] It usually consumes a large amount of energy to regulate indoor supercooling or overheating. Energy issues have become a popular topic in recent years. Most energy conversions are dependent on non-renewable resources such as petroleum and gasoline for a long time.[2,3] With the decrease in non-renewable energy and the increased demand for energy consumption, looking for alternative renewable resources is one of the important research directions in the energy field.[4,5] At present, many scholars have conducted research on renewable energy such as solar energy,[6] wind energy,[7] tidal energy[8], and geothermal energy.[9] What's more, some excellent renewable energy sources have been widely used in production and application. Among them, solar energy is been widely studied and applied because of its convenience, low cost, clean, and environmentally friendly features. In building energy, converting solar energy into heat energy is an eco-friendly and common way. However, due to the instability of solar energy acquisition, such as light intensity, light time, light area, *etc.*, the conversion of pure solar energy into thermal energy is not matched in time and space, causing a low utilization rate.

Phase change materials (PCMs) control physical state change by absorbing and releasing energy, alleviating the time-space mismatch during energy conversion. Compared to inorganic PCMs, Organic PCMs have great advantages among numerous PCMs, such as high phase change enthalpy, good circulation, non-toxicity, and so on.[10-12] Paraffin (PW), as an organic material with stable performance, not only meets all the above advantages but also shows great properties such as easy access, low price, and high latent heat storage.[13] However, pure PCMs without fixed structures are easy to leak during physical state conversion, which is not conducive to practical application.[14] Therefore, extreme performance can not be performed when the pure PW working.[15,16] Embed PCMs into framework materials with porous or three-dimensional network structures to prepare composite PCMs (CPCMs) is a common method to solve these problems.[17–19] CPCMs, regarded as one of the most important materials to solve energy problems,[20–22] which achieve PCMs widespread applications in the energy field, are the major focus of current energy research.[23–27] Common frame support materials

[1] *School of Materials and Energy, Guangdong University of Technology, Guangzhou 510006, China.*
[2] *Key Laboratory of Polymer Processing Engineering (South China University of Technology), Ministry of Education, Guangzhou, 510640, China.*
E-mail: jintao.huang@gdut.edu.cn (J. Huang), ygmin@gdut.edu.cn (Y. Min)

include polyethylene,[28] polypropylene,[29] polyurethane,[30] polylactic acid,[31], *etc*. Selecting appropriate frame materials can improve PCMs quality, prevent leakage and maintain shape stability.[17,32] CPCMs applied as building exterior materials are an environmental-friendly way to alleviate the increasing building consumption. In addition to stable and excellent photothermal conversion efficiency, as a superior building exterior material, it is necessary to show outstanding hydrophobicity, acid corrosion resistance, and thermal insulation. Remarkably, the functional demand for building materials was increased by COVID-19 spreading.[33] People may be attracted and prefer to use some antimicrobial materials with disinfected functions.[34] However, ordinary polymer materials are difficult to meet the above requirements. Polyimide (PI) is one of the most outstanding organic polymers and exhibits the most excellent comprehensive properties[35] including acid corrosion resistance, high-temperature resistance,[36] excellent mechanical properties, anti-aging,[37] hydrophobic[38], and other properties. Shuge Peng *et al*. have verified that the modified polyimide–silver nanoparticle–ceramic composite membrane has lasted for antibacterial and anti-biofouling performance.[39] PI aerogels also show advantageous properties (lightweight, porous holes, and good thermal insulation). Some scholars have prepared polyimide aerogels by compounding with montmorillonite,[40] graphene,[41] aramid fiber[42], and other materials. PI aerogels have been applied in oil-absorbing,[43] heat insulation,[44] hydrophobic[45] and other fields.

In this study, a series of CPCMs with good energy storage performance, acid resistance, hydrophobicity, and antimicrobial resistance were prepared, which have great application in environmentally friendly building exterior wall materials. Polyimide aerogels and PW were composited to prepare CPCMs. PI aerogels formed by different PI molecular structures exhibited different properties. The PI formed by 3,3',4,4'-biphenyltetracarboxylic dianhydride-1,4-phenylenediamine (BPDA-PPD) chains has good hydrophobic properties.[46] In this paper, BPDA-PPD chains were crosslinked by 1,3,5-Benzene tricarboxylic acid chloride to form a three-dimensional network structure. BPDA-4,4′-oxidianiline (ODA) formed linear PI molecules. Semi-interpenetrating polyimide aerogels were prepared by crosslinking PI and linear PI. The morphology and pore size of framework aerogels were tunable by controlling the ratio of both PI molecules. PW was then encapsulated in aerogels by vacuum impregnation. The energy storage performance and cycle stability of CPCMs were verified. Also, acid corrosion resistance, hydrophobicity, and antimicrobial resistance of CPCMs were studied.

2. Experimental section

2.1 Chemical and materials

3,3',4,4'-Biphenyl tetracarboxylic dianhydride (BPDA), p-Phenylenediamine (PPD), N-Methylpyrrolidone (NMP, 99.5%) and Triethylamine (TEA, 99.5%) were purchased from Shanghai Macklin Biochemical Co., Ltd. 4,4'-oxydianiline (ODA, 99%) was supplied by Changzhou Sunlight Medical Raw Material Co., Ltd. 1,3,5-Benzene tricarboxylic acid chloride (BTC, 98%) was obtained from Accela ChemBio Co., Ltd. PW wax bought from Shanghai Aladdin Biochemical Technology Co., Ltd.

2.2 Characterization

Microstructure of aerogels and their CPCMs was observed by Hitachi SU8220 scanning electron microscope (SEM). PI aerogels and their CPCMs were characterized by The Fourier transform infrared (FT-IR) spectra (Nicolet 6700). XRD measurements were performed by X-ray diffraction (XRD) (XRD, D/MAX-Ultima IV). Thermogravimetric Analysis (TGA) was tested by using a thermal gravimetric analyzer (TGA/DSC 3+/1600HT, Mettler Toledo). The melting and freezing information of CPCMs were investigated by differential scanning calorimetry (DSC, DSC8000, PerkinElmer), heating, and cooling at a rate of 10 °C/min between 0 and 100 °C under a nitrogen atmosphere. Light absorption characteristics were studied by UV-visible spectroscopy (LAMBDA 950, Perkin Elmer, USA). The laser flash system (Netzsch LFA 447) was used to measure the thermal diffusivity of materials. Thermal images were recorded with a Smart Sensor infrared camera (285-220S-68, Fotric). The water contact angle (WCA) was measured by a static contact angle instrument (OCA 15 plus, Germany) at room temperature. Detailed information on antimicrobial resistance was provided in "Supporting Information (SI)".

2.3 Preparation

2.3.1 Aerogel preparation

Different kinds of 10 wt.% polyamic acids (PAA) solutions were prepared under an N_2 atmosphere. Put PPD and BPDA (n_{PPD}: n_{BPDA} = 1.05:1) into NMP solution stirring for 12 h, and then gained PAA_1. Dropped TEA into PAA_1 (n_{PPD}: n_{TEA} = 1:3) and stirred for 6 h. BTC was added into the mixture stirring for 1 h to gain PAA_{s1} mixture. The resultant mixture was mixed into acetone with a light yellow solid precipitating out. The solid was dried in an oven at 60 °C for 12 h, named PAA_{s1}.

Put ODA and BPDA (Noda: n_{BPDA} = 1:1.01) into NMP solution stirring for 12 h, and then gained PAA_2. Weighed and added TEA into PAA_2 (Noda: n_{TEA} = 1:3) and stirred for 6 h to gain PAA_{s2} mixture. The mixture was dropped into acetone gaining the other yellow solid, which also dried at 60 °C for 1 h and called PAA_{s2}.

The preparation of aerogel and its CPCMs is shown in Fig. 1. All aerogels were prepared by changing the mole ratio between PAA_{s1} and PAA_{s2} (n_{PPD} = 100%, 75%, 25%, and 0). PAA_{s1} and PAA_{s2} were added into deionized water to prepare the mixture, and then all mixtures were frozen overnight. All samples are freeze-dried for 48 h to gain PAA aerogels. These aerogels were imidized after being heated at 250 °C and 350 °C for 10 mins, respectively. Then, PI aerogels were obtained. For discussion convenience, these aerogels are named as P_xO_y,

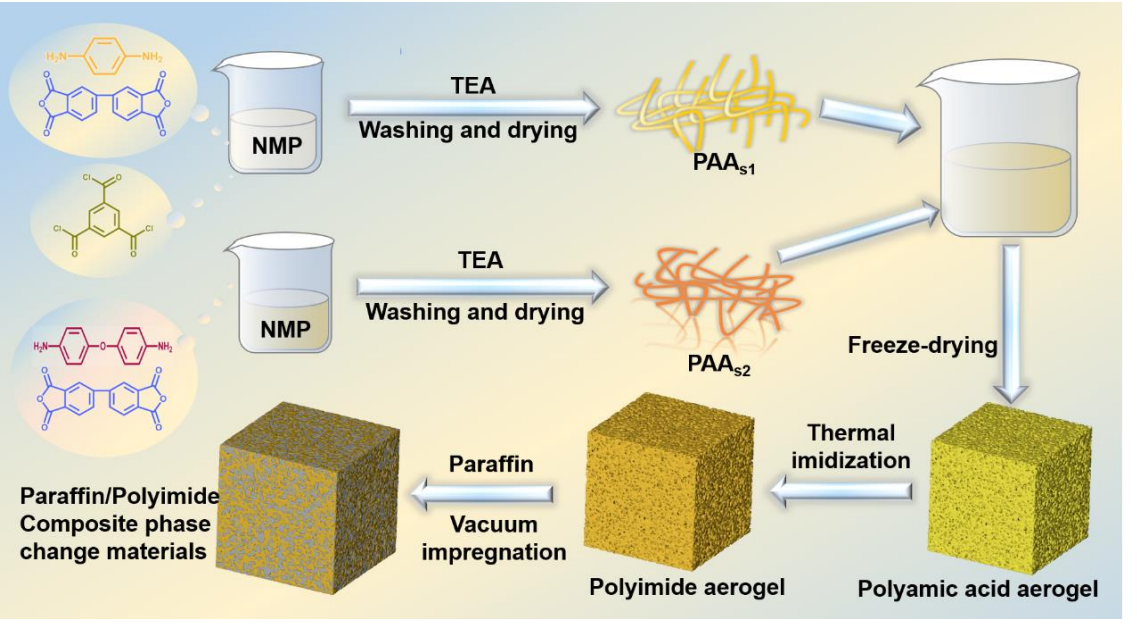

Fig. 1 The schematic diagram of CPCMs preparation.

and x is the mole content of PPD in aerogel, y is that of ODA. According to this rule, these samples were called $P_{100}O_0$, $P_{75}O_{25}$, $P_{50}O_{50}$, $P_{25}O_{75}$, and P_0O_{100}.

2.3.2 Composite phase change materials preparation

All aerogel samples were vacuum impregnated in the molten PW for 24h. The leaking test was performed, and finally, CPCMs were gained. For discussion convenience, all composite materials are named P-P_XO_Y.

3. Results and discussion

3.1 Properties of CPCMs

Leaking tests of all CPCMs were performed. The specific leaking process was shown in Fig. 2. At first, excess PW without being completely fixed is separated from PCMs and transferred to the filter paper. The filter paper is replaced every two hours until no leakage of PW existed on the filter paper. The load of PW (W_f) is based on the equation:

$$W_f = \frac{m_1 - m_0}{m_1} \times 100\% \quad (1)$$

In this equation, m_1 is the mass of CPCMs, and m_0 is the mass of the pure PI aerogel.

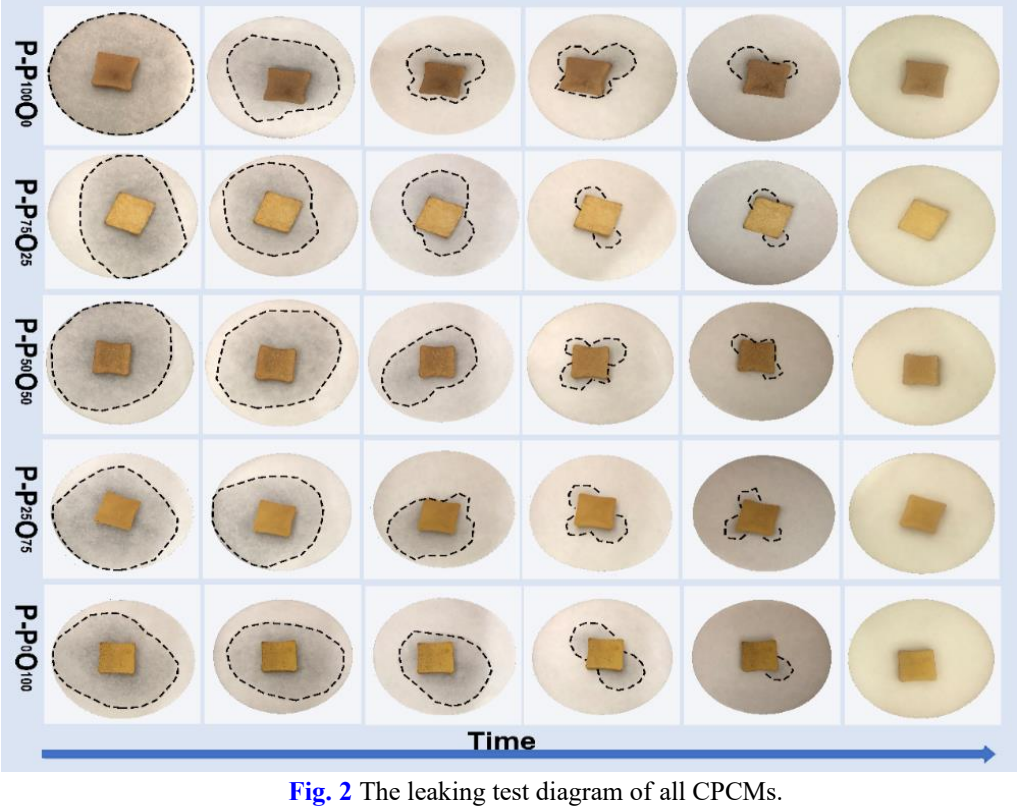

Fig. 2 The leaking test diagram of all CPCMs.

Table 1. The load of PW of all PCMs.

Sample	P-$P_{100}O_0$	P-$P_{75}O_{25}$	P-$P_{50}O_{50}$	P-$P_{25}O_{75}$	P-P_0O_{100}
W_f(%)	83.0	76.0	47.7	47.2	74.1

The loading capacity of each sample is shown in Table 1. The PW loading of P-$P_{50}O_{50}$ and P-$P_{25}O_{75}$ is 47.7% and 47.2%, respectively, which are much lower than that of others. In other samples, PI aerogels as frame materials maintain good dimensional stability, and there is no extreme and huge difference in PW adsorption.

The SEM images of PI aerogels and their CPCMs are shown in Fig. 3. As shown in Figs. 3(a-e), PI aerogels prepared from BPDA-PPD chains combined by BTC, form a three-dimensional crosslinking structure. The size of the porous structure shrinks as the linear molecular stacking of BPDA-ODA increases. $P_{50}O_{50}$ and $P_{25}O_{75}$ exhibit layer structures with small holes. P_0O_{100} shows the common layer structure as made by the freezing-drying way. Three-dimensional crosslinking bonds and the interlayer gap provide a huge chance for PW absorption. As shown in Figs. 3(f-j), PW is embedded in the porous structure of frame materials and their interlayer gap. As for $P_{50}O_{50}$ and $P_{25}O_{75}$, their holes are too small to fix PW. Therefore, PW can only be fixed in the layer, causing lower absorption than others.

The FT-IR images of PI aerogels, PW, and their CPCMs are shown in Figs. 4(a, d). As shown in Fig. 4(a), all PI samples exhibit characteristic peaks of PI, including 1370 cm^{-1}(C-N), 1720 cm^{-1}(C=O), 1780 cm^{-1}(C=O), and 1500 cm^{-1}(the symbol of benzene).[47,48] Notably, there is no observed 1238 cm^{-1} and 1170 cm^{-1} in $P_{100}O_0$, and the intensity of these two peaks is changed by the content of ODA in other samples.[49] PW shows peaks in 2950 cm^{-1}(-CH_3), 2910 cm^{-1} and 2850 cm^{-1}(C-H), 1460 cm^{-1}(C-H).[50] In Fig. 4(d), the same peaks are obtained in all samples which were only different in their intensities. There is no new peak obtained, so it is confirmed that PW did not connect with PI aerogels in the chemical method.

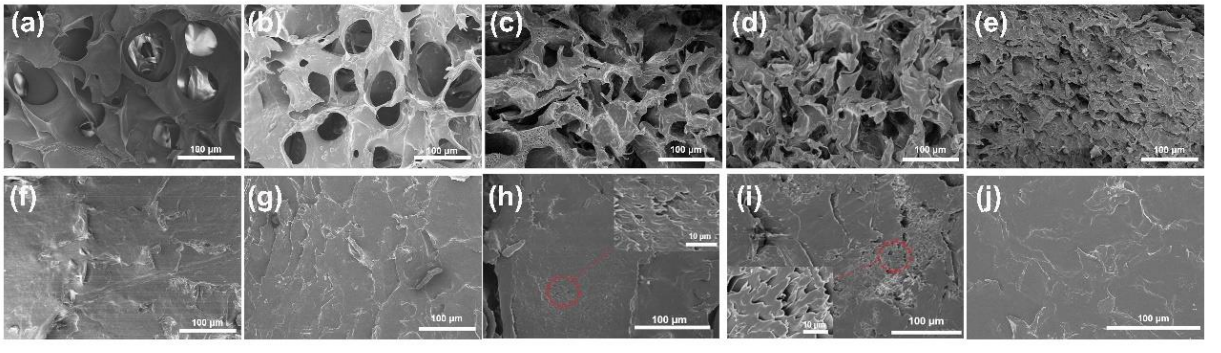

Fig. 3 SEM images of (a) $P_{100}O_0$; (b) $P_{75}O_{25}$; (c) $P_{50}O_{50}$; (d) $P_{25}O_{75}$; (e) P_0O_{100}; (f) P- $P_{100}O_0$; (g) P-$P_{75}O_{25}$; (h) P-$P_{50}O_{50}$; (i) P-$P_{25}O_{75}$; (j) P-P_0O_{100}.

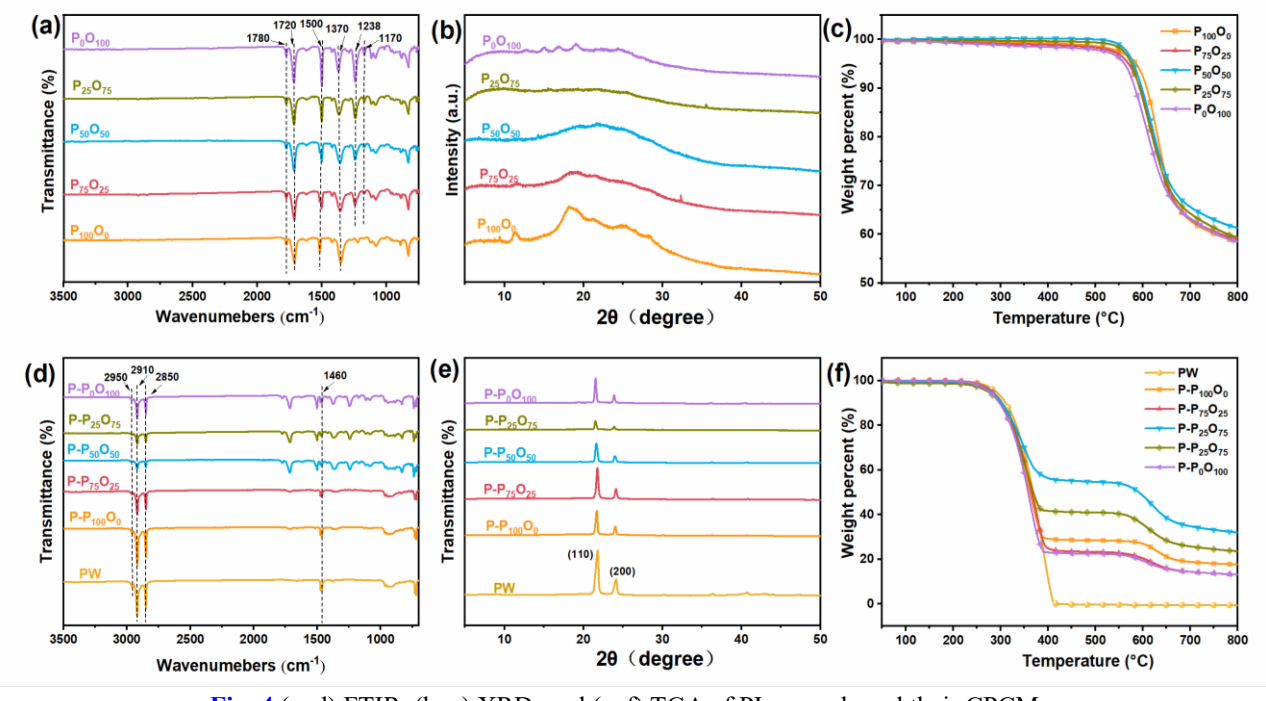

Fig. 4 (a, d) FTIR, (b, e) XRD, and (c, f) TGA of PI aerogels and their CPCMs.

The XRD testing results are shown in Figs. 4(b, e). the characteristic peaks of PI aerogels are changed by PI types, demonstrating these PI chains are amorphous or microcrystalline. The angle of 21.78°(110) and 24.12°(200) are exhibited in PW.[51] In Fig. 4(e), there are not any new peaks occurred, confirming that PI aerogel did not composite with PW via chemical linking. But at the same time, the (110) and (200) crystal peaks from CPCMs left shift and their width becomes narrow. Due to the restriction of the PI framework, the crystal size of PW chains is affected and reduced.

The TGA results are shown in Figs. 4(c, f). Commonly, the decomposition temperature (T_d) of PI prepared by high reactivity diamine (PPD) is expected to be higher than that of PI prepared by ODA.[20] As shown in Fig. 4(c), the range of $T_{d10\%}$ decomposition temperature is between 582 to 608 °C. Therefore, PI aerogels show outstanding thermal stability and are beneficial to preparing stable cycling CPCMs. In Fig. 4(f), PW is completely decomposed and volatilized at 416 °C. The weight loss of CPCMs is roughly consistent with the PW absorption of all CPCMs. In addition, CPCMs have hard weight loss within 100 °C and show excellent thermal stability.

3.2 The transformation of composite phase change materials

Outstanding CPCMs show high heating conversion capability. As shown in Figs. 5(a, b), the phase change temperature and latent heat of pure PW and its CPCMs are measured by DSC analysis. All related data about DSC results are listed in Table 2. T_m and T_f are represented by the melting or crystallinity temperature of PW and CPCMs, respectively. It is clear to observe a small heating peak and a sharp heating peak when these samples stay in the temperature heating from 0 °C to 100 °C. The small heating peak is observed by the solid-solid phase transition of PW, while the sharp one is caused by the solid-liquid phase transition.[50] As shown in Table 2, the $T_{m(on)}$ and $T_{f(on)}$of PW are 47.4 °C and 42.3 °C, respectively. $T_{m(on)}$ of all CPCMs was higher than that of pure PW and $T_{f(on)}$ was lower than that of PW. ΔT_m and ΔT_f were different with different PI aerogels.

ΔH_m and ΔH_f are the meltings and freezing enthalpy of CPCMs and pure PW. The melting enthalpy of pure PW is 142.07 J/g and its freezing enthalpy is 137.14 J/g. According to equations:

$$\alpha = \frac{\Delta H_{m(P-P_xO_y)}}{\Delta H_{m(PW)}} \times 100\% \quad (2)$$

$$\eta = \frac{\Delta H_{m(P-P_xO_y)}}{\Delta H_{m(PW)} \times W_f} \times 100\% \quad (3)$$

α is the theoretical enthalpy efficiency. η is the relative enthalpy efficiency. The theoretical and relative enthalpy efficiencies of all CPCMs are shown in Figs. 5(c, d). P-$P_{100}O_0$, P-$P_{75}O_{25}$, and P-P_0O_{100} show excellent enthalpy efficiency performance and their enthalpy efficiency is more outstanding than other CPCMs listed in Table 3. In addition, the theoretical values of P-$P_{50}O_{50}$ and P-$P_{25}O_{75}$ are extremely lower than their relative values. This main be caused by their low loading.[52]

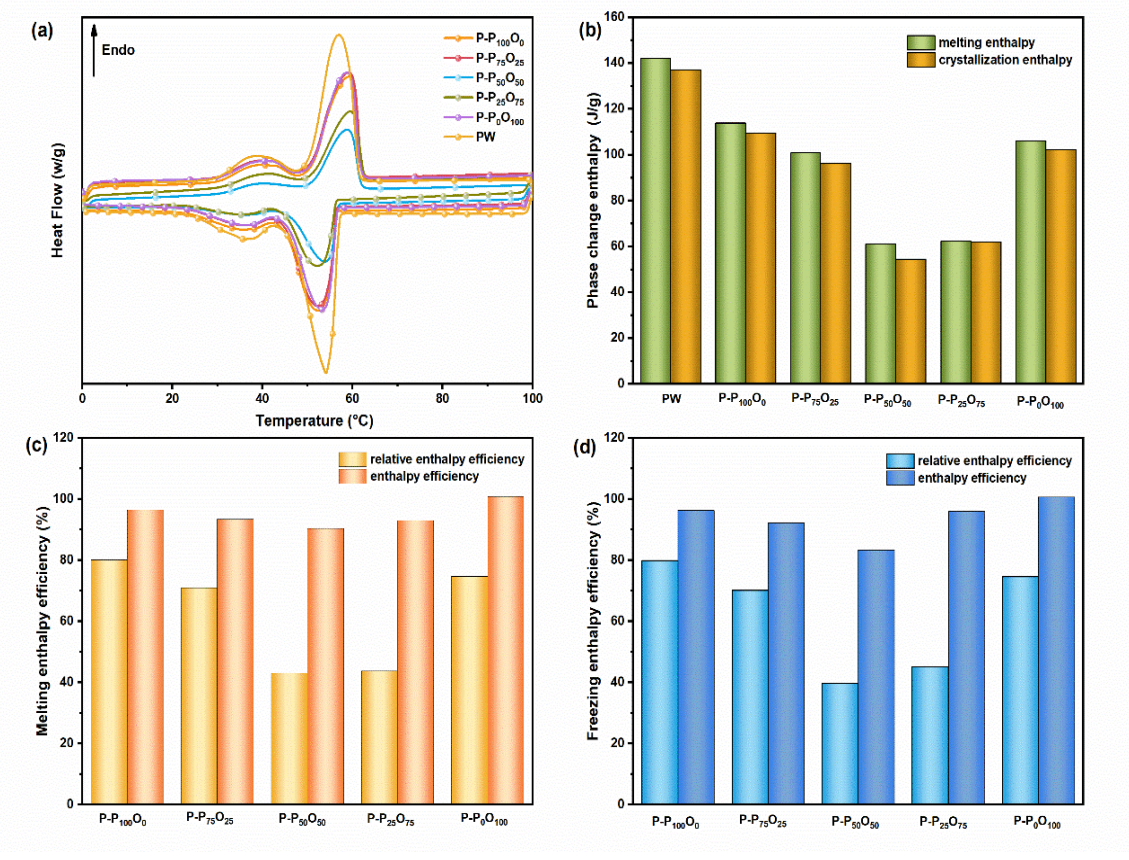

Fig. 5 (a) DSC curves and (b) the latent heat of PW and CPCMs. (c, d) The efficiency of CPCMs.

Table 2. The melting and freezing temperature values of pure PW and CPCMs.

Samples	$T_{m(on)}$ (°C)	T_m (°C)	$T_{m(end)}$ (°C)	ΔT_m (°C)	$T_{f(on)}$ (°C)	T_f (°C)	$T_{f(off)}$ (°C)	ΔT_f (°C)
PW	47.4	57.0	63.2	15.8	57.7	54.2	42.3	20.9
P-$P_{100}O_0$	47.7	59.2	64.0	16.3	57.0	52.4	41.9	22.1
P-$P_{75}O_{25}$	47.7	58.2	64.4	16.7	57.1	54.0	41.2	23.2
P-$P_{50}O_{50}$	48.4	58.2	63.9	15.5	57.5	53.7	42.3	21.6
P-$P_{25}O_{75}$	47.9	59.2	64.5	16.6	56.8	52.7	41.9	22.6
P-P_0O_{100}	47.7	58.8	63.9	16.2	57.5	53.4	42.1	21.8

Table 3. Some α and η values of CPCMs reported in other articles.

Refs	PW-based PCMS	Melting process		Freezing Process	
		α (%)	η (%)	α (%)	η (%)
This article	P-$P_{100}O_0$	80.2	96.6	80.0	96.3
	P-$P_{75}O_{25}$	71.1	93.5	70.2	92.3
	P-$P_{50}O_{50}$	43.1	90.4	39.8	83.5
	P-$P_{25}O_{75}$	43.9	93.0	45.3	96.0
	P-P_0O_{100}	74.8	100.9	74.6	100.7
[53]	PW/EG/cement	16.8	56.0	23.0	76.7
[51]	Octadecane/VMT	62.8	77.91	52.1	64.7
[19]	PW/CAN800	57.7	96.2	53.4	89
[54]	PW/PVC	14.0	15	14.6	15.0
[55]	PW/HDPE	24.0	26.2	23.0	26.2
[56]	PW/ASA/SEBS	38.6	77.2	38.3	76.6

3.3 Cycle stability

200 heating-cooling cycle experiments were conducted to verify the thermal cycle stability of P-$P_{100}O_0$, P-$P_{75}O_{25}$, and P-P_0O_{100}. These PCMs were put into a thermostatic drying oven with the cycling temperature raising from 0 °C to 100 °C and kept for 5 min, and then decreasing to 0 °C. DSC curves of PCMs before and after 200 thermal cycles are shown in Figs 6(a-c). The ΔH_m and the ΔH_f of before and after cycling samples are listed in Table 4. Relative coefficients (δ_m and δ_f) were sited to evaluate the loss of ΔH_m and the ΔH_f after cycling. The lower δ_m and δ_f are, the more outstanding cycle stability is. According to equations:

$$\delta_m = \frac{\Delta H_m(before) - \Delta H_m(after)}{\Delta H_m(before)} \times 100\ \% \quad (4)$$

$$\delta_f = \frac{\Delta H_f(before) - \Delta H_f(after)}{\Delta H_f(before)} \times 100\ \% \quad (5)$$

Table 4. Thermal parameters of PCMs before and after 200 thermal cycles.

Samples		ΔH_m (J/g)	δ_m (%)	ΔH_f (J/g)	δ_f (%)
P-$P_{100}O_0$	Before	113.89	-	109.65	-
	after	106.85	6.18	105.70	3.60
P-$P_{75}O_{25}$	Before	100.98	-	96.21	-
	after	96.69	4.25	95.51	0.73
P-P_0O_{100}	Before	106.21	-	102.37	-
	after	94.15	11.35	89.17	12.89

As shown in Table 4, the loss ratio of P-$P_{100}O_0$ was the highest. It may be caused by its huge hole structure. These huge holes are easy to absorb but unbeneficial to encapsulating PW. Therefore, PW is easy to escape from the framework material in the cycling heating process. P-P_0O_{100} shows the middle loss ratio. Also, the layer structure is suitable to absorb PW but may not be conducive to storage. The P-$P_{75}O_{25}$ change of melting or freezing enthalpy is minimal, from 100.98 to 96.69 J/g, and 96.21 to 95.51 J/g, respectively. At the same time, the loss ratio of melting or freezing enthalpy is 4.25% and 0.73%, respectively, which performed more excellent cycling stability than other PCMs shown in Table 5.

XRD and FTIR results of PCMs before and after 200 thermal cycles are shown in Figs. 6(d-i). There are no significant changes in characteristic peaks among PCMs before and after 200 thermal cycles. These phenomena also indicate the excellent cycle stability of PI aerogel as framework material combined with PW. All these results show that PCMs composited by PI aerogel and PW have a great wide application in the thermal storage field.

Table 5. The loss ratio of PCMs reported in others research.

Refs	Sample	Cycle	δ_m (%)	δ_f (%)
[57]	PW/epoxy/EG	1	6.5	-
[58]	EG/PW/Silicone	20	27.1	26.5
[59]	PW/HDPE/EG	100	5.69	3.53
[60]	PW/biocarbon	200	11.1	3.93
This work	P-$P_{100}O_0$	200	6.18	3.60
	P-$P_{75}O_{25}$	200	4.25	0.73
	P-P_0O_{100}	200	11.35	12.89

3.4 Photothermal conversion

Figure 7(a) UV-vis spectra of P-$P_{75}O_{25}$ and PW; (b) the simulation diagram of the photothermal conversion device, where Sp1, Sp2, and Sp3 correspond to P-$P_{75}O_{25}$, $P_{75}O_{25}$, and PW.

The UV-vis absorption intensity spectrum of pure PW and P-$P_{75}O_{25}$ is shown in Fig. 7(a). In this wavelength range, the absorption of pure PW is extremely low, with only a weak absorption peak between 200-400 nm. However, the light absorption performance of CPCM with PI as the frame material is improved. The higher the light absorption capacity, the stronger the light-to-heat conversion efficiency. This means that the PI frame material not only provides good frame support for CPCM but also helps to improve its light response performance, beneficial to effectively absorbing light and

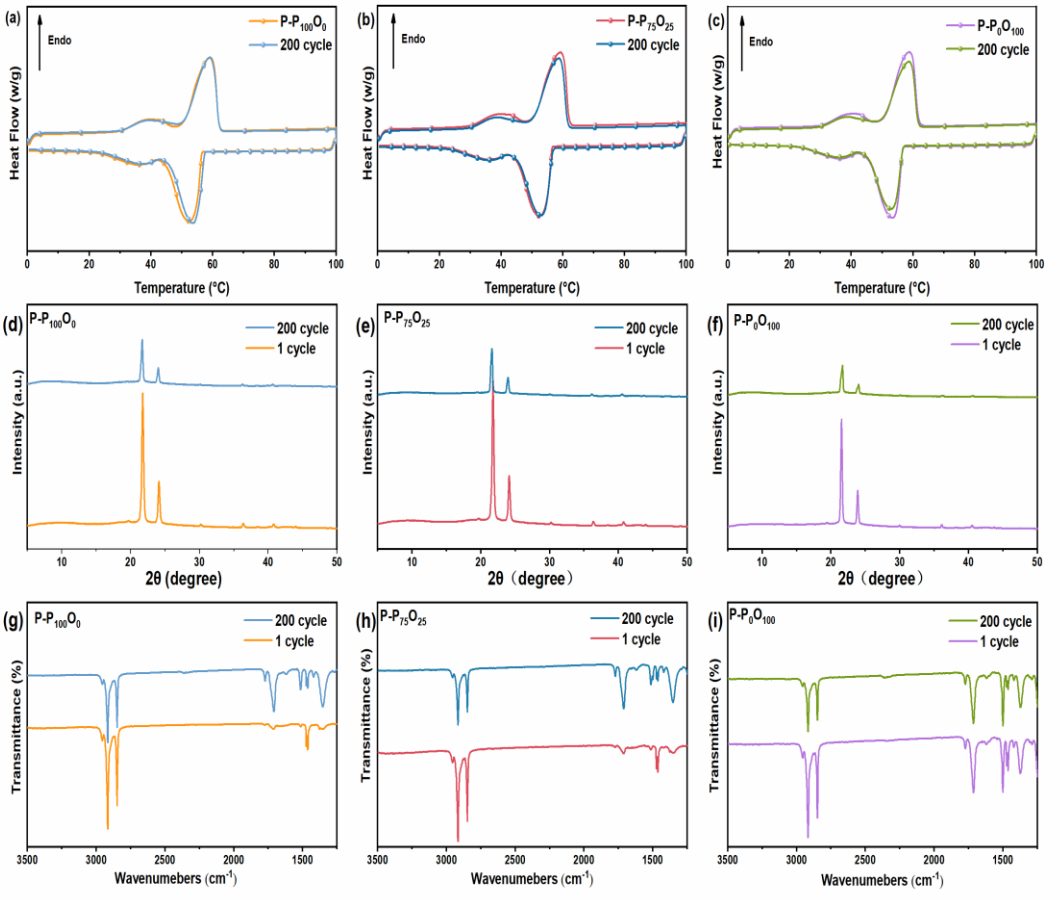

Fig. 6 (a-c) DSC curves, (d-f) XRD, and (g-i) FTIR of P-$P_{100}O_0$, P-$P_{75}O_{25}$, P-P_0O_{100}.

converting it to heat.[61]

The photo-thermal conversion simulation was carried out with the device shown in Fig. 7(b). Fig. 8 shows the thermal management of PW (Sp1), P-$P_{75}O_{25}$ (Sp2), and $P_{75}O_{25}$ (Sp3) under different time points. In Fig. 8, the part in low temperature is shown in a blue-black area and that in high temperature was indicated in an orange-yellow or even white area. At the beginning (Fig. 8(a)), the temperature of all samples is so near room temperature. Their corresponding temperature-time curves are exhibited in Fig. 9(a). As the temperature rises quickly to the electric device's heating, the detected temperature of $P_{75}O_{25}$ is higher than others. It may be caused by the worse thermal conductivity of $P_{75}O_{25}$. The heat accumulates on the aerogel surface under simulated solar light irradiation, so its surface temperature is the highest. Due to the poor lighting absorption,[62] the temperature of PW rises slowly and is 56.9 °C eventually. In the contrast, the heating on P-$P_{75}O_{25}$ can be conducted by the solid-solid phase transition, so the heat spreads rapidly to the whole and the surface temperature rises slowly in a short time. The melting point of PW is between 60 to 62 °C, and at this time, P-$P_{75}O_{25}$ is converting solid-liquid phase transition to storage corresponding melting enthalpy. After heating for under 1000 s, the temperature of P-$P_{75}O_{25}$ is higher than 62 °C, which has finished the solid-liquid phase transition. The temperature of P-$P_{75}O_{25}$ still rises slowly until the end of simulated solar light,

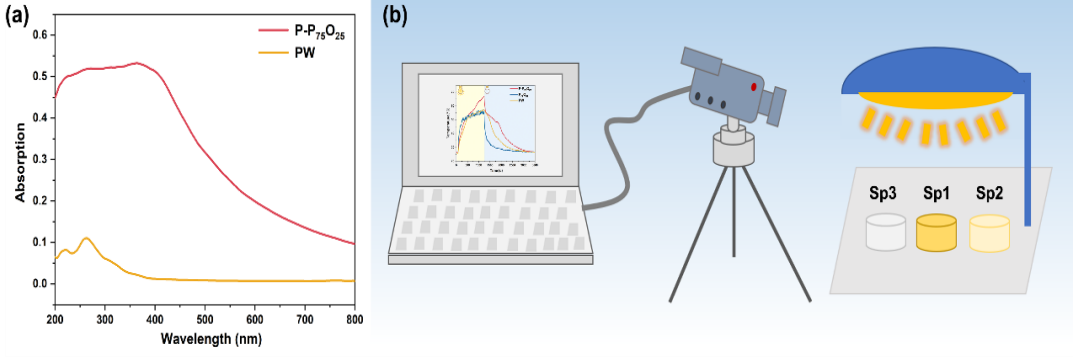

Fig. 7 (a) UV-vis spectra of P-$P_{75}O_{25}$ and PW; (b) the simulation diagram of the photothermal conversion device, where Sp1, Sp2, and Sp3 correspond to P-$P_{75}O_{25}$, $P_{75}O_{25}$, and PW.

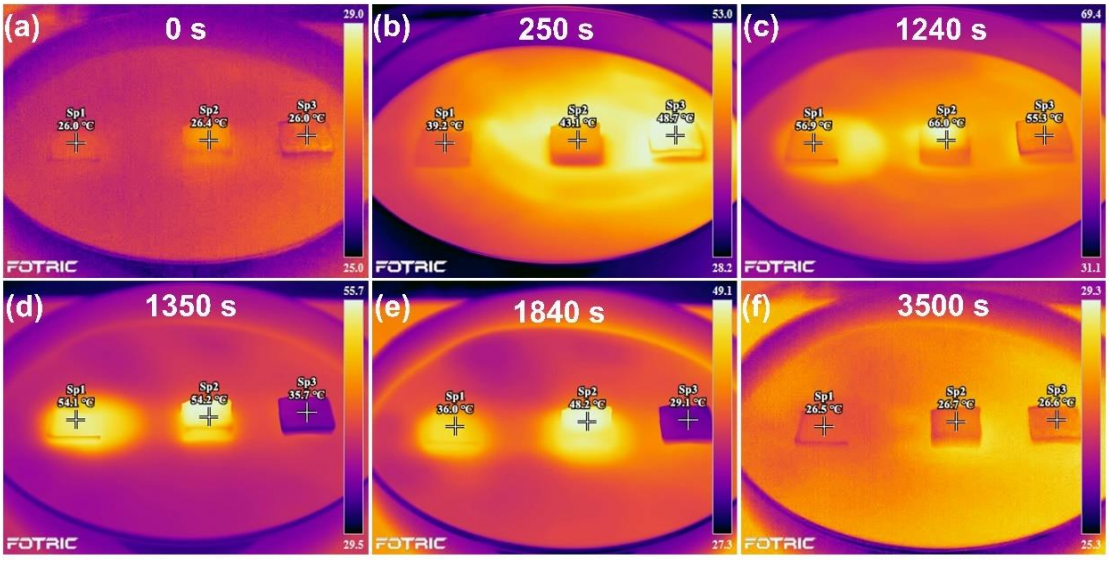

Fig. 8 The thermal infrared photographs of thermal management.

reaches the maximal value. The temperature of $P_{75}O_{25}$ is still at 55.3 ºC because of its poor thermal diffusivity. The electric devices turn off under 1350 s.

When $P_{75}O_{25}$ does not absorb heat from the external heat source, the heat accumulated on the surface is quickly dissipated and its temperature drops quickly. In the contrast, PW and P-$P_{75}O_{25}$ undergo a liquid-solid phase transition and release the corresponding latent heat of solidification so their surface temperature drops slowly. The temperature of P-$P_{75}O_{25}$ delays slower 2000 seconds than that of $P_{75}O_{25}$ to be the same as room temperature. Compared with pure PW, an isotherm platform occurs in P-$P_{75}O_{25}$, which has an advantage in thermal insulation field application. Therefore, P-$P_{75}O_{25}$ shows great performance on photothermal conversion and has high heating energy storage ability.

The relative thermal conductivity is shown in Fig. 9(b). The thermal conductivity of PI aerogel is extremely low and its CPCM still shows low thermal conductivity (0.253 W/(m·K)). It is beneficial to prolong the thermal insulation process with the combination of its lower thermal conductivity and higher latent heat. Storing energy by natural lighting instead of a large amount of additional energy consumption, P-$P_{75}O_{25}$ has great potential in the application of high-performance building materials.

3.5 Hydrophobic and insulation performances

The water contact angle (WCA) was measured to verify the hydrophobic property of P-$P_{75}O_{25}$. PI aerogel has a great performance in hydrophobic and acid corrosion resistance fields. To imitate the phenomena of acid rain corrosion, P-$P_{75}O_{25}$ was dropped into a solution (pH = 5.6) for 5 and 10 min. The WCA of these samples was tested as shown in Fig. 10. The WCA of P-$P_{75}O_{25}$ is near 131.9° (Fig. 10(a)). Other acid-treated samples showed hydrophobic property and their WCA (Figs. 10 (b, c)) are similar to that of the original sample. P-$P_{75}O_{25}$ still shows great hydrophobic stability even in an acid environment.

Meanwhile, the self-cleaning and antifouling ability of P-$P_{75}O_{25}$ is shown in Figs. 10 (d-f). the whole process is reported in "Supporting Information (SI)". Water droplets are easy to

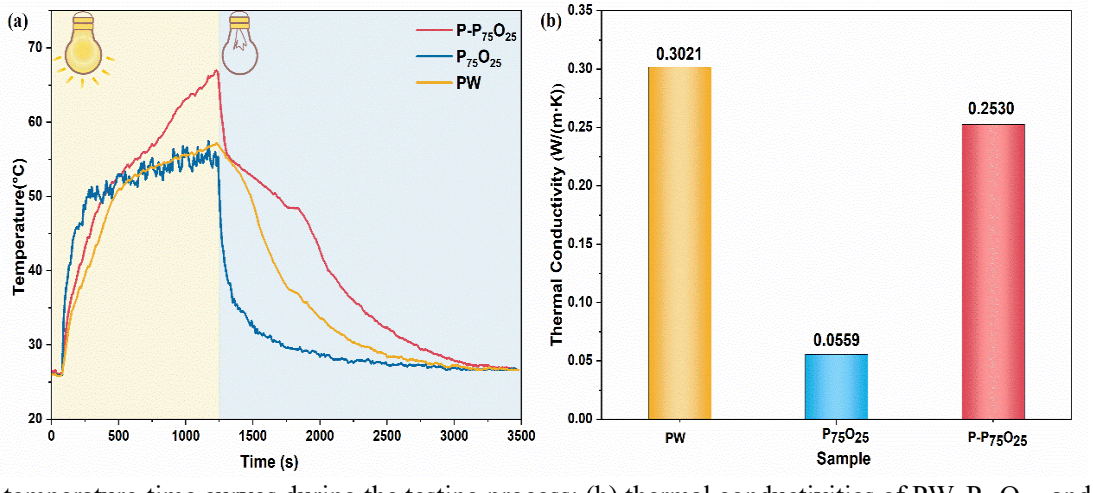

Fig. 9 (a) The temperature-time curves during the testing process; (b) thermal conductivities of PW, $P_{75}O_{25}$, and P-$P_{75}O_{25}$.

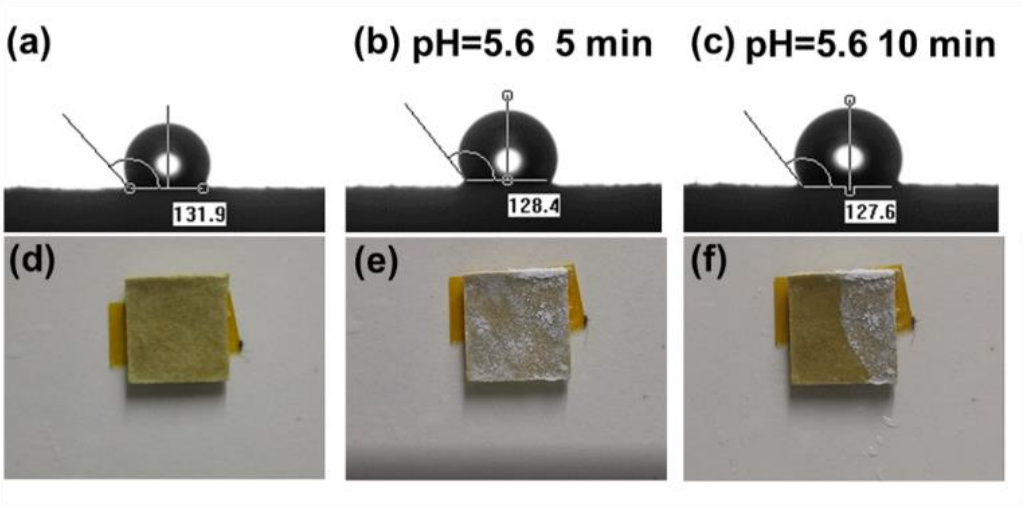

Fig. 10 The water contact angle of P-$P_{75}O_{25}$. (a) The normal condition; (b) drowned in the acid solution for 5 min; (c) drowned in the acid solution for 10 min. (d) the original P-$P_{75}O_{25}$ aerogel, (e) the dusty P-$P_{75}O_{25}$ aerogel and (f) self-cleaning antifouling experiment for P-$P_{75}O_{25}$.

combine with dust on the surface of P-$P_{75}O_{25}$, rolling down and removing dust. In the realistic, adhesive bacteria on the wall may be washed away when the water dropped. The hydrophobic self-cleaning wall has a positive effect on the antimicrobial.[63,64]

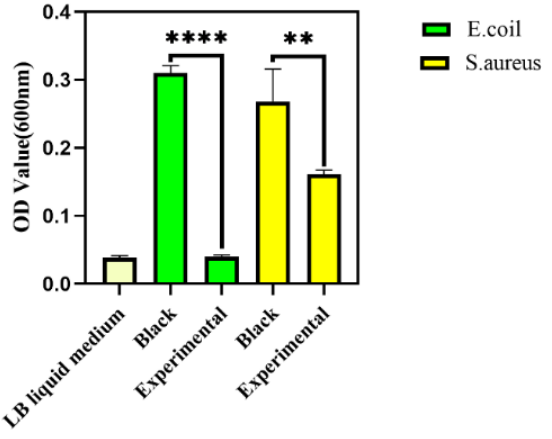

Fig. 11 The intuitive data of all suspensions.

The antimicrobial activity of P-$P_{75}O_{25}$ was also verified. The specific materials and methods are exhibited in "Supporting Information (SI)". As shown in Fig. 11, the optical density value gained from the experimental group is lower than that prepared from the blank one in each contrast system. These results confirmed the antimicrobial effect of P-$P_{75}O_{25}$, which is beneficial to maintaining stable properties. P-$P_{75}O_{25}$ integrates excellent acid resistance, hydrophobic, self-cleaning, and antimicrobial performance, exhibiting outstanding light-thermal conversion capacity and cycling stability, which has a wide aspect in the environmental-friendly construction material field.

4. Conclusions

In this research, a series of CPCMs with excellent comprehensive properties is prepared by PW and PI aerogel as framework material. PI aerogel provides a great packaging performance. Among all CPCMs, P-$P_{75}O_{25}$ ($n_{(BPDA\text{-}PPD)}$:$n_{(BPDA\text{-}ODA)}$ = 75:25) shows the best property. The mass fraction of PW in P-$P_{75}O_{25}$ is 76.0 wt.%. The latent heat of P-$P_{75}O_{25}$ during melting and freezing is 100.98 J/g and 96.21 J/g, respectively. The relative enthalpy efficiencies of P-$P_{75}O_{25}$ during melting and freezing are 93.5% and 92.3%, respectively. The latent heat values of P-$P_{75}O_{25}$ after the 200 thermal cycle is similar to that before. The loss of melting and freezing enthalpies are 4.25% and 0.73%, respectively, which verified that P-$P_{75}O_{25}$ has good thermal reliability and reusability. At the same time, it shows excellent hydrophobicity, acid corrosion resistance, and antimicrobial resistance. Therefore, P-$P_{75}O_{25}$ has great application potential in the environmental-friendly building field, especially as a lighting-thermal, hydrophobic, self-cleaning, and antimicrobial wall material.

Acknowledgments

This research was funded by the National Natural Science Foundation of China (Grant No. 52003111 and U20A20340), the National Key R&D Program of China (2020YFB0408100), the Program for Guangdong Introducing Innovative and Entrepreneurial Team (2016ZT06C412), the Opening Project of Key Laboratory of Polymer Processing Engineering (South China University of Technology), Ministry of Education, (Grant No. KFKT2001), Key-Area Research and Development Program of Guangdong Province (2020B010182001).

Conflict of Interest

The authors declare no conflict of interest.

Supporting information

Applicable.

References

[1] R. Zeinelabdein, S. Omer, G. Gan, *Renewable and Sustainable Energy Reviews*, 2018, **82**, 2843-2868, doi: 10.1016/j.rser.2017.10.046.

[2] X. Lu, J. Huang, W. Wong, J. Qu, *Solar Energy Materials and Solar Cells*, 2019, **200**, 109987, doi: 10.1016/j.solmat.2019.109987.

[3] W. Deng, L. Deng, Z. Li, Y. Zhang, G. Chen, *ACS Applied Materials & Interfaces*, 2021, **13**, 12131-12140, doi: 10.1021/acsami.1c01059.

[4] J. Huang, Y. Luo, M. Weng, J. Yu, L. Sun, H. Zeng, Y. Liu, W. Zeng, Y. Min, Z. Guo, *ES Materials and Manufacturing*, 2021, **13**, 23-39, doi: 10.30919/esmm5f458.

[5] J. Huang, S. Lyu, H. Han, Y. Wang, H. Sun, J. Su, Y. Liu, Y. Min, D. Sun, *Energy*, 2022, **252**, 123962, doi: 10.1016/j.energy.2022.123962.

[6] Y. Du, H. Huang, X. Hu, S. Liu, X. Sheng, X. Li, X. Lu, J. Qu, *Renewable Energy*, 2021, **171**, 1-10, doi: 10.1016/j.renene.2021.02.077.

[7] J. Praene, D. Fakra, F. Benard, L. Ayagapin, M. Rachadi, *Renewable Energy*, 2021, **169**, 885-893, doi: 10.1016/j.renene.2021.01.067.

[8] L. Liu, C. Liu, Z. Sun, *Renewable and Sustainable Energy Reviews*, 2011, **15**, 1089-1097, doi: 10.1016/j.rser.2010.11.022.

[9] T. Li, H. Qin, J. Wang, X. Gao, N. Meng, Y. Jia, Q. Liu, *Renewable Energy*, 2021, **175**, 318-336, doi: 10.1016/j.renene.2021.04.062.

[10] M. Umair, Y. Zhang, K. Iqbal, S. Zhang, B. Tang, *Applied Energy*, 2019, **235**, 846-873, doi: 10.1016/j.apenergy.2018.11.017.

[11] X. Hu, H. Wu, S. Liu, S. Gong, Y. Du, X. Li, X. Lu,J. Qu, *Engineered Science*, 2022, **17**, 1-27, doi: 10.30919/es8d474.

[12] J. Tao, J. Luan, Y. Liu, D. Qu, Z. Yan, X. Ke, *Renewable and Sustainable Energy Reviews*, 2022, **159**, 112175, doi: 10.1016/j.rser.2022.112175.

[13] R. Gulfam, P. Zhang, Z. Meng, *Applied Energy*, 2019, **238**, 582-611, doi: 10.1016/j.apenergy.2019.01.114.

[14] M. Santamouris, G. Yun, *Renewable Energy*, 2020, **161**, 792-807, doi: 10.1016/j.renene.2020.07.109.

[15] N. Sarier, E. Onder, *Thermochimica Acta*, 2012, **540**, 7-60, doi: 10.1016/j.tca.2012.04.013.

[16] W. Su, J. Darkwa, G. Kokogiannakis, *Renewable and Sustainable Energy Reviews*, 2015, **48**, 373-391, doi: 10.1016/j.rser.2015.04.044.

[17] G. Abdeali, A. Bahramian, M. Abdollahi, *Journal of Energy Storage*, 2020, **29**, 101299, doi: 10.1016/j.est.2020.101299.

[18] Y. Qu, J. Chen, L. Liu, T. Xu, H. Wu, X. Zhou, *Renewable Energy*, 2020, **150**, 1127-1135, doi: 10.1016/j.renene.2019.10.073.

[19] X. Zuo, J. Li, X. Zhao, H. Yang, D. Chen, *Renewable Energy*, 2020, **152**, 579-589, doi: 10.1016/j.renene.2020.01.087.

[20] S. Zhang, W. Hu, D. Li, C. Zhang, M. Arıcı, Ç. Yıldız, X. Zhang, Y. Ma, *Energy*, 2021, **222**, 119916, doi: 10.1016/j.energy.2021.119916.

[21] P. Rathore, S. Shukla, *Energy and Buildings*, 2021, **236**, 110799, doi: 10.1016/j.enbuild.2021.110799.

[22] A. Rai, *Building and Environment*, 2021, **199**, 107930, doi: 10.1016/j.buildenv.2021.107930.

[23] Y. Qu, D. Zhou, F. Xue, L. Cui, *Energy and Buildings*, 2021, **241**, 110966, doi: 10.1016/j.enbuild.2021.110966.

[24] X. Lu, H. Liu, V. Murugadoss, I. Seok, J. Huang, J. Ryu, Z. Guo, *Engineered Science*, 2020, **9**, 25-34, doi: 10.30919/es8d901.

[25] Y. Liu, M. Xie, X. Gao, Y. Yang, Y. Sang, *Applied Thermal Engineering*, 2018, **140**, 112-119, doi: 10.1016/j.applthermaleng.2018.05.042.

[26] R. Ye, W. Lin, K. Yuan, X. Fang, Z. Zhang, *Applied Energy*, 2017, **193**, 325-335, doi: 10.1016/j.apenergy.2017.02.049.

[27] D. Pan, G. Yang, H. Abo-Dief, J. Dong, F. Su, C. Liu, Y. Li, B. Xu, V. Murugadoss, N. Naik, S. El-Bahy, Z. El-Bahy, M. Huang, Z. Guo, *Nano-Micro Letters*, 2022, **14**, 118, doi: 10.1007/s40820-022-00863-z.

[28] X. Hu, H. Wu, X. Lu, S. Liu, J. Qu, *Advanced Composites and Hybrid Materials*, 2021, **4**, 478-491, doi: 10.1007/s42114-021-00300-6.

[29] H.Hong, Y. Pan, H. Sun, Z. Zhu, C. Ma, B. Wang, W. Liang, B. Yang, An Li, *Solar Energy Materials and Solar Cells*, 2018, **174**, 307-313, doi: 10.1016/j.solmat.2017.09.026

[30] C. Amaral, S. Pinto, T. Silva, F. Mohseni, J. Amaral, V. Amaral, P. Marques, A. Timmons, R. Vicente, *Journal of Energy Storage*, 2020, **28**, 101177, doi: 10.1016/j.est.2019.101177.

[31] Y. Li, Z. Lin, X. Wang, Z. Duan, P. Lu, S. Li, D. Ji, Z. Wang, G. Li, D. Yu, W. Liu, *Separation and Purification Technology*, 2021, **270**, 118794, doi: 10.1016/j.seppur.2021.118794.

[32] L. Navarro, A. Gracia, D. Niall, A. Castell, M. Browne, S. McCormack, P. Griffiths, L. Cabeza, *Renewable Energy*, 2016, **85**, 1334-1356, doi: 10.1016/j.renene.2015.06.064.

[33] S. Ducoli, A. Zacco, E. Bontempi, *Journal of Environmental Management*, 2021, **282**, 111966, doi: 10.1016/j.jenvman.2021.111966.

[34] B. Yu, N. Li, C. Yan, X. Liu, H. Liu, J. Ji, X. Xu, *Renewable Energy*, 2022, **182**, 1201-1218, doi: 10.1016/j.renene.2021.11.029.

[35] B. Shi, B. Ma, C. Wang, H. He, L. Qu, B. Xu, Y. Chen, *Composites Part A: Applied Science and Manufacturing*, 2021, **143**, 106283, doi: 10.1016/j.compositesa.2021.106283.

[36] Y. Lin, C. Chen, S. Hu, D. Zhang, G. Wu, *Journal of Materials Research and Technology*, 2020, **9**, 10719-10731, doi: 10.1016/j.jmrt.2020.07.075.

[37] D. Zhang, Y. Lin, W. Wang, Y. Li, G. Wu, *Applied Surface Science*, 2021, **543**, 148833, doi: 10.1016/j.apsusc.2020.148833.

[38] X. Zhang, W. Li, P. Song, B. You, G. Sun, *Chemical Engineering Journal*, 2020, **381**, 122784, doi: 10.1016/j.cej.2019.122784.

[39] S. Peng, Y. Chen, X. Jin, W. Lu, M. Gou, X. Wei, J. Xie, *Journal of Membrane Science*, 2020, **611**, 118340, doi: 10.1016/j.memsci.2020.118340.

[40] N. Zhang, H. Guo, L. Xiong, H. Zhang, X. Chen, *Journal of Energy Storage*, 2021, **34**, 102189, doi: 10.1016/j.est.2020.102189.

[41] C. Zhan, S. C. Jana, *Microporous and Mesoporous Materials*,

2020, **307**, 110501, doi: 10.1016/j.micromeso.2020.110501.
[42] Y. Wang, Y. Cui, Z. Shao, W. Gao, W. Fan, T. Liu, H. Bai, *Chemical Engineering Journal*, 2020, **390**, 124623, doi: 10.1016/j.cej.2020.124623.
[43] X. He, L. Zhang, D. Meng, J. Wu, *European Polymer Journal*, 2017, **89**, 461-467, doi: 10.1016/j.eurpolymj.2017.02.039.
[44] J. Kwon, J. Kim, D. Park, H. Hana *Polymer*, 2015, **56**, 68-72, doi: 10.1016/j.polymer.2014.06.090.
[45] Z. Wu, B. Han, C. Zhang, D. Zhu, Z. Yang, *Polymer*, 2019, **179**, 121605, doi: 10.1016/j.polymer.2019.121605.
[46] J. Seo, H. Han, *Polymer Degradation and Stability*, 2002, **77**, 477-482, doi: 10.1016/s0141-3910(02)00105-2.
[47] M. Weng, L. Jian, X. Feng, X. Luo, J. Hu, J. Zhang, Y. Liu, Y. Min, *Ceramics International*, 2021, **47**, 24519-24526, doi: 10.1016/j.ceramint.2021.05.170.
[48] Y. Wang, Y. Yang, Z. Jia, J. Qin, Y. Gu, *Polymer*, 2012, **53**, 4157-4163, doi: 10.1016/j.polymer.2012.07.034.
[49] S. Mosanenzadeh, Z. Saadatnia, F. Shi, C. Park, H. Naguib, *Polymer*, 2019, **176**, 213-226, doi: 10.1016/j.polymer.2019.05.050.
[50] M. Maleki, P. Ahmadi, H. Mohammadi, H. Karimian, R. Ahmadi, H. Emrooz, *Solar Energy Materials and Solar Cells*, 2019, **191**, 266-274, doi: 10.1016/j.solmat.2018.11.022.
[51] O. Chung, S. Jeong, S. Kim, *Solar Energy Materials and Solar Cells*, 2015, **137**, 107-112, doi: 10.1016/j.solmat.2014.11.001.
[52] X. Li, X. Sheng, Y. Guo, X. Lu, H. Wu, Y. Chen, L. Zhang, J. Gu, *Journal of Materials Science & Technology*, 2021, **86**, 171-179, doi: 10.1016/j.jmst.2021.02.009.
[53] L. Liu, J. Chen, Y. Qu, T. Xu, H. Wu, G. Huang, X. Zhou, L. Yang, *Solar Energy Materials and Solar Cells*, 2019, **200**, 110038, doi: 10.1016/j.solmat.2019.110038.
[54] X. Jin, J. Li, P. Xue, M. Jia, *Solar Energy Materials and Solar Cells*, 2014, **130**, 435–441, doi: 10.1016/j.solmat.2014.07.013.
[55] M. Karkri, M. Lachheb, Z. Nógellová, B. Boh, B. Sumiga, M. A. AlMaadeed, A. Fethi, I. Krupa, *Energy and Buildings*, 2015, **88**, 144-152, doi: 10.1016/j.enbuild.2014.11.061.
[56] B. Xiang, Z. Yang, J. Zhang, *Polymers for Advanced Technologies*, 2021, **32**, 420–427, doi: 10.1002/pat.5097.
[57] Z. Wang, W. Situ, X. Li, G. Zhang, Z. Huang, W. Yuan, C. Yang, C. Yang, *Applied Thermal Engineering*, 2017, **123**, 1006-1012, doi: 10.1016/j.applthermaleng.2017.05.179.
[58] Y. Zhang, W. Li, J. Huang, M. Cao, G. Du, *Materials*, 2020, **13**, 894, doi: 10.3390/ma13040894.
[59] Y. Xie, Y. Yang, Y. Liu, S. Wang, X. Guo, H. Wang, D. Cao, *Advanced Composites and Hybrid Materials*, 2021, **4**, 543-551, doi: 10.1007/s42114-021-00249-6.
[60] Y. Xu, X. Zhang, Z. Huang, G. Chen, G. Leng, F. Lin, W. Zhang, Y. Liu, M. Fang, X. Wu, X. Min, *ChemistrySelect*, 2020, **5**, 12051-12056, doi: 10.1002/slct.202001270.
[61] Y. Shao, W. Hu, M. Gao, Y. Xiao, T. Huang, N. Zhang, J. Yang, X. Qi, Y. Wang, *Composites Part A: Applied Science and Manufacturing*, 2021, **143**, 106291, doi: 10.1016/j.compositesa.2021.106291.
[62] L. Cheng, L. Kong, X. Zhang, X. Kong, *Solar Energy Materials and Solar Cells*, 2022, **235**, 111461, doi: 10.1016/j.solmat.2021.111461.
[63] K. Ellinas, D. Kefallinou, K. Stamatakis, E. Gogolides, A. Tserepi, *ACS Applied Materials & Interfaces*, 2017, **9**, 39781-39789, doi: 10.1021/acsami.7b11402.
[64] J. Ma, C. Liu, K. Yan, *Chemical Engineering Journal*, 2022, **429**, 132170, doi: 10.1016/j.cej.2021.132170.

Author Information

Mengman Weng *is currently a PH.D. Candidate in South China university of technology. She received her bachelor degree in 2019 and master degree in 2022 from Guangdong University of technology. Her research interests mainly focus on the preparation and application of functional polyimide materials.*

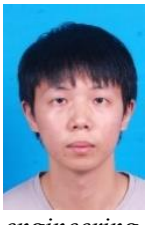

Shengdong Liu *is currently a PH.D. Candidate under the supervision of Prof. Yonggang Min in Guangdong University of Technology. He received his bachelor degree in 2020 from East China Jiaotong University. His research interests mainly focus on bone tissue engineering, conductive degradable biomaterials, and antibacterial materials.*

Jintao Huang *obtained his bachelor degree in 2009 and master degree in 2012 from Sichuan University, and doctor degree in 2015 from South China University of Technology. Now, he is an associate professor in Guangdong University of Technology. His research focuses on the preparation and performance of bio-based energy materials and the preparation of energy storage materials by traditional processing methods.*

Yonggang Min *obtained his Ph.D. from Professor Alan G. MacDiarmid at University of Pennsylvania in 1995, and then had worked various technical positions among several global fortune 500 companies and Universities. Now, he is a professor in Guangdong University of Technology. Professor Min had a strong academic training and industrial experience in carbon based materials, electric active polymers, and polymeric materials. He had published over 130 technical papers (citation over 3000), filed over 200 patents, and conducted about 100 technical presentations worldwide*

Publisher's Note: Engineered Science Publisher remains neutral with regard to jurisdictional claims in published maps and institutional affiliations.